ISSN 1674-1056
http://cpb.iphy.ac.cn
http://iopscience.iop.org/cpb
中国物理 B
Chinese Physics
中国物理 Chinese Physics B

Effects of bismuth on structural and dielectric properties of cobalt-cadmium spinel ferrites fabricated via micro-emulsion route

Furhaj Ahmed Sheikh, Muhammad Khalid, Muhammad Shahzad Shifa, H M Noor ul Huda Khan Asghar, Sameen Aslam, Ayesha Perveen, Jalil ur Rehman, Muhammad Azhar Khan, Zaheer Abbas Gilani

Citation: Chin. Phys. B . 2019, 28(8): 088701. **doi:** 10.1088/1674-1056/28/8/088701
Journal homepage: http://cpb.iphy.ac.cn; http://iopscience.iop.org/cpb

What follows is a list of articles you may be interested in

Structure instability-induced high dielectric properties in[001]-oriented $0.68Pb(Mg_{1/3}Nb_{2/3})O_3$-$0.33PbTiO_3$crystals

Xiao-Juan Li(李晓娟), Xing Fan(樊星), Zeng-Zhe Xi(惠增哲), Peng Liu(刘鹏), Wei Long(龙伟), Pin-Yang Fang(方频阳), Rui-Hua Nan(南瑞华)
Chin. Phys. B . 2019, 28(5): 057701. **doi:** 10.1088/1674-1056/28/5/057701

Characterization of vertical Au/β -Ga_2O_3 single-crystal Schottky photodiodes with MBE-grown high-resistivity epitaxial layer

X Z Liu(刘兴钊), C Yue(岳超), C T Xia(夏长泰), W L Zhang(张万里)
Chin. Phys. B . 2016, 25(1): 017201. **doi:** 10.1088/1674-1056/25/1/017201

High performance trench MOS barrier Schottky diode with high-*k* gate oxide

Zhai Dong-Yuan, Zhu Jun, Zhao Yi, Cai Yin-Fei, Shi Yi, Zheng You-Liao
Chin. Phys. B . 2015, 24(7): 077201. **doi:** 10.1088/1674-1056/24/7/077201

Electrical bistable devices using composites of zinc sulfide nanoparticles and poly-(N-vinylcarbazole)

Cao Ya-Peng, Hu Yu-Feng, Li Jian-Tao, Ye Hai-Hang, Lü Long-Feng, Ning Yu, Lu Qi-Peng, Tang Ai-Wei, Lou Zhi-Dong, Hou Yan-Bing, Teng Feng
Chin. Phys. B . 2015, 24(3): 037201. **doi:** 10.1088/1674-1056/24/3/037201

Effects of A1 site occupation on dielectric and ferroelectric properties of $Sr_4CaRTi_3Nb_7O_{30}$ (*R*=Ce, Eu) tungsten bronze ceramics

Fang Yu-Jiao, Gong Gao-Shang, Gebru Zerihun, Yuan Song-Liu
Chin. Phys. B . 2014, 23(12): 128701. **doi:** 10.1088/1674-1056/23/12/128701

Effects of bismuth on structural and dielectric properties of cobalt-cadmium spinel ferrites fabricated via micro-emulsion route

Furhaj Ahmed Sheikh[1], Muhammad Khalid[1], Muhammad Shahzad Shifa[2], H M Noor ul Huda Khan Asghar[1], Sameen Aslam[1], Ayesha Perveen[1], Jalil ur Rehman[1], Muhammad Azhar Khan[3], and Zaheer Abbas Gilani[1,†]

[1] *Department of Physics, Balochistan University of Information Technology, Engineering & Management Sciences, Quetta* 87300, *Pakistan*
[2] *Department of Physics, Government College University, Faisalabad* 38000, *Pakistan*
[3] *Department of Physics, The Islamia University of Bahawalpur* 63100, *Pakistan*

(Received 22 March 2019; revised manuscript received 12 June 2019; published online 25 July 2019)

Spinel ferrites have a significant role in high-tech applications. In the present work nano-crystalline ferrites having general formula $Co_{0.5}Cd_{0.5}Bi_xFe_{2-x}O_4$ with ($x = 0.0$, 0.05, 0.1, 0.15, 0.2, and 0.25) are synthesized via micro-emulsion route. Powder x-ray diffraction (XRD) studies discover the FCC spinel structure. Crystalline size is calculated in a range of 11 nm–15 nm. Lattice parameter calculations are reduced due to its substitution which leads to the exchange of large ionic radius of Fe^{3+} for small ionic radius of Bi^{3+}. The x-ray density is analyzed to increase with doping. Fourier transform infrared spectroscopy (FTIR) is performed to analyze absorption band spectra. The two absorption bands are observed in a range of 400 cm^{-1}–600 cm^{-1}, and they are the characteristic feature of spinel structure. Thermo-gravimetric analysis (TGA) reveals the total weight loss of nearly 1.98%. Dielectric analysis is carried out by impedance analyzer in a frequency span from 1 MHz to 3 GHz by using the Maxwell Wagner model. Dielectric studies reveal the decrease of dielectric parameters. The alternating current (AC) conductivity exhibits a plane behavior in a low frequency range and it increases with the applied frequency increasing. This is attributed to the grain effects in a high frequency range or may be due to the reduction of porosity. Real and imaginary part of impedance show the decreasing trend which corresponds to the grain boundary action. The imaginary modulus shows the occurrence of peak that helps to understand the interfacial polarization. Cole-Cole graph shows a single semicircle which confirms that the conduction mechanism is due to the grain boundaries at low frequency. Dielectric studies reveal the applicability of these ferrites in high frequency equipment, microwave applications, high storage media, and semiconductor devices.

Keywords: Co-ferrite, nanocrystalline ferrites, XRD, microemulsion, dielectric properties

PACS: 87.19.rf, 72.20.–I, 77.84.–s, 47.54.Jk **DOI:** 10.1088/1674-1056/28/8/088701

1. Introduction

Ferrites are the materials containing iron oxide as its main component, and they are ferromagnetic oxides possessing high permeability and resistivity.[1] They have vast area of applications in all the fields because they are suitable for the applications in high frequency, resistivity and high corrosion resistance.[2] Their commercial use appeared after 1950 in electronic devices like computer circuitry, microwave devices, television, telephones, radio, magnetic memories and transformers and so on. The ferrites possess a large number of bulk applications but the phenomenon of magnetism lies in nano-scale domain.[3] Spinel ferrites have great significance because of their electrical and dielectric characteristics, and these characteristics depend on the chemical composition and the method of preparation. Recently, with the development in information technology, high performance storage devices have received great attention.[4] Multiferroic materials have significance due to their ferroelectric, ferromagnetic and ferroelastic properties. The application of external electric field, magnetic field and stress can cause the change in spontaneous magnetization, polarization and deformation, respectively. Mutual coupling of these phenomena has revealed their applications in sensing, storage and spintronic devices {Wang, 2019 #135}.[5–7] The ferrites possess characteristics of behaving like inhomogeneous dielectric material consisting of highly conducting grains detached by air gap or insulating layers called grain boundaries.[8] Dielectric properties of ferrite like dielectric constant, tangent loss, AC conductivity and impedance can be controlled by annealing and composition.[9,10] Nowadays cobalt ferrites gained much attention due to their applications in high electromagnetic, industrial and biomedical applications. They have good electromagnetic properties and hardness just because of their high chemical stability.[11–13] The characteristics of these ferrites greatly depend on synthesis methodology and the annealing temperature. It should be noted that size of such ferrites strictly relies on annealing temperature.[14–21] In a current refined era, a limited number of researches have been done on cobalt–cadmium spinel ferrites, and researchers have paid magnificent attention to the DC electrical conductivity which exhibits an increasing trend with the rise of temperature.[22]

†Corresponding author. E-mail: zagilani2002@yahoo.com, zaheer.abbas@buitms.edu.pk

© 2019 Chinese Physical Society and IOP Publishing Ltd

Researchers have also reported the increase in conductance characteristics of cobalt–cadmium ferrites as well as catalytic decomposition of 2-propanol. The cobalt-cadmium ferrites with variational composition, magnetic coupling leads to a strengthening effect on A–B interaction.[14] Research groups have also reported an increase in dielectric properties of material as well as AC conductivity.[23]

In the present study, the cobalt-cadmium ferrite having bismuth as a substituent are prepared via micro-emulsion route. The prepared ferrite material is characterized by thermo-gravimetric analysis (TGA), x-ray diffraction (XRD), Fourier transform infrared spectroscopy (FTIR) and dielectric properties analysis.

2. Experimental technique

Bismuth substituted cobalt–cadmium ferrites were manufactured by micro-emulsion technique. The general composition formula used was $Co_{0.5}Cd_{0.5}Bi_xFe_{2-x}O_4$ ($x = 0.0$, 0.05, 0.1, 0.15, 0.2, and 0.25). The materials used were cobalt (II) nitrate hexa-hydrate (Co $(No_3)_2.6H_2O$), cadmium nitrate tetra-hydrate (Cd $(No_3)_2.4H_2O$), bismuth (III) nitrate penta-hydrate (Bi $(No_3)_3.5H_2O$), ferric (III) nitrate nano-hydrate (Fe $(No_3)_3.9H_2O$), and cetyl trimethyl ammonium bromide (CTAB) $C_{19}H_{42}NBr$. The sample solutions were prepared and in order to make the homogenous mixture and hot plate magnetic stirrer was used. The prepared ferrites samples were characterized by using TGA/DTA analysis to study the weight loss of material with respect to the provided temperature. The XRD was carried out on PANalytical XPert Pro to analyze the crystal structure and to find several parameters pertaining to the crystalline structure. The value of 2θ was set to be in a range from 10 ° to 80 °. The FTIR analysis was done on iS50 FT-IR to investigate tetrahedral and octahedral stretching bands. The dielectric analysis was done by impedance analyzer to investigate the dielectric properties of prepared ferrite material. Several dielectric parameters like dielectric constant, dielectric loss, tangent loss, AC conductivity, real and imaginary part of impedance and modulus are calculated in frequency range from 1-MHz to 3-GHz range, their variations are studied with the increase of Bi^{3+} content as well.

3. Results and discussion

3.1. TGA-DTA analysis

Thermo-gravimetric analysis (TGA) as well as differential thermal analysis (DTA) of prepared sample $Co_{0.5}Cd_{0.5}Fe_2O_4$ is accomplished in a temperature range of 0 °C–1010 °C. The analysis of percentage weight loss against temperature was made with the help of TGA curve, which exhibits that the decomposition process is completed step by step.

A weight loss of about 1.98% is observed in the whole temperature range. Rapid changes in the curve occur at 55 °C and 420 °C. Below 100 °C there is a weight loss of approximately 0.38%, which is due to the evaporation of water.[24,25] At 358 °C the weight loss of about 1.38% occurs which is due to the decomposition of matter, evaporation of water and oxidation of organic matter.[26,27] Secondly, most of the weight loss is nearly 1.36% occurring in the temperature range of 100 °C–420 °C. Then in the last step, a 0.17% weight loss is found in the temperature range of 420 °C–974 °C. From TGA graph it follows that the phase formation starts at 900 °C after which there is very small weight loss, beyond 1010 °C there exists no weight loss, which confirms the creation of stable phase. The DTA curve shows that the decomposition is carried out step by step due to some exothermic peaks. The first sharp peak is observed at 94 °C, the second oneoccurs at 234 °C and the third one appears at 405 °C, indicating the burning of additional constituents.[24,28] Figure 1 shows the TGA and DTA curves.

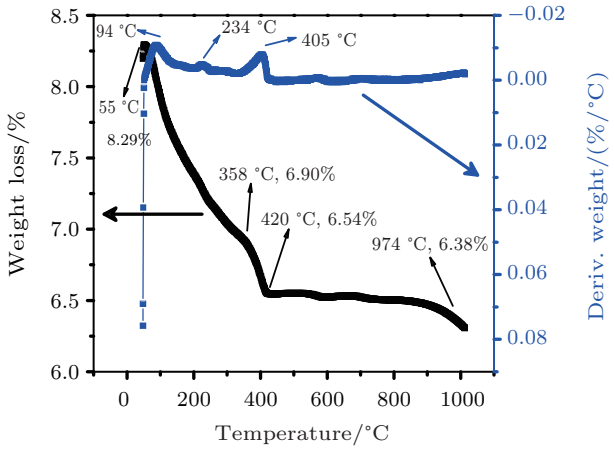


Fig. 1. TGA and DTA curves.

3.2. XRD analysis

Bismuth doped cobalt–cadmium ferrites having general composition formula $Co_{0.5}Cd_{0.5}Bi_xFe_{2-x}O_4$ ($x = 0.0$, 0.05, 0.1, 0.15, 0.2, and 0.25) are synthesized via micro-emulsion route. To study the crystalline structure in detail and identify the crystalline phase formation, powder XRD is carried out on PANalytical XPert Pro.[29] It is very basic and important characterization technique to determine certain parameters of crystal structure like, crystalline size, lattice constant, bulk density, x-Ray density, stacking fault, lattice strain, micro-strain and dislocation density, and so on. The crystalline phase of the material is confirmed because the obtained XRD pattern consists of very sharp peaks. At $2\theta = 35°$ the most intense peaks are observed to have 311 *hkl* value, this peak is considered to be an ideal for cubic structure.[30] The peaks corresponding to XRD pattern are studied and are indexed as (220), (311), (222), (400), (422), (511), (440), (531), and (533). These peaks correspond to the FCC spinel structure.[31,32] For further confirmation, these peaks are verified by JCPDS card number 22-1086. A couple of impure peaks has also been observed: one is at $2\theta = 44.5°$ having *hkl* value 411, the other is at $2\theta = 32.9°$ in the sixth sample indicated by (*). The occurrence of these peaks may be because of insolubility of Bi at octahedral site.[26,33] The XRD patterns of the synthesized ferrite samples are shown in Fig. 2.

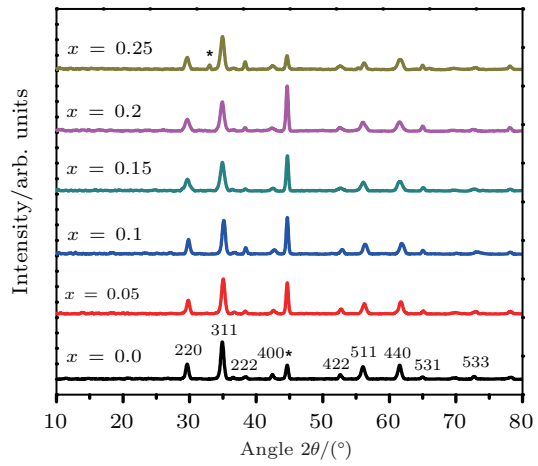


Fig. 2. XRD Analysis of $Co_{0.5}Cd_{0.5}Bi_xFe_{2-x}O_4$ ($x = 0.0$, 0.05, 0.1, 0.15, 0.2, and 0.25).

The crystalline size is calculated for the *hkl* value of (311) from the Debye Sherrer's formula given by

$$D_m = \frac{k\lambda}{\beta \cos\theta}, \tag{1}$$

where k is the constant having a valueof 0.9, λ is the x-ray beam wavelength and its value is 1.54 Å, β is the full width at half maximum (FWHM) of the (311) peak, and θ is its angle of diffraction.[4] The crystalline size varies in homogenously with the substitution of Bi. This behavior of inhomogeneity existing in crystalline size may be due to the generation of secondary phase and also relatively small ionic radius of Bi^{3+} as compared with that of the Fe^{3+} which is to be replaced.[26] Lattice constant is calculated by Nelson Relay Function. This is given as follows:

$$a = d\sqrt{(h^2+k^2+l^2)}. \tag{2}$$

The average lattice constant is calculated to be in a range of 8.46 Å–8.5 Å. The variations in the "a" is described on the basis of Bi^{3+} and Fe^{3+} ion radius. Lattice parameter is found to decrease with the substitution of Bi ion content.

This is due to the replacement of large radius of Fe^{3+} ion (0.76 Å) by smaller radius of Bi^{3+} ion (0.74 Å) at the octahedral site.[34–36] Lattice constant first decreases rapidly with the substitution and then increases, in the end it again decreases, which s may be due to the segregation of Bi^{3+} ions on grain boundaries.[1] The x-ray density of synthesized ferrite is found from the following formula:

$$\rho_x = 8M/Na^3, \tag{3}$$

where M represents the molecular weight, N the Avogadro number, and a^3 is a unit cell volume. The relation between x-ray density and concentration is almost linear. With the increase of Bi^{3+} concentration, the x-ray density also increases: this is attributed to the greater molar weight of Bi^{3+} (208.98) than that of Fe^{3+} (55.845). Bulk density of the prepared pallets is calculated from the formula

$$\rho_m = \frac{m}{v}, \tag{4}$$

where m represents the mass of pallet and 'v' its volume. Lattice strain (ε) of the prepared nanoparticles is calculated from the Stokes–Wilson equation

$$\varepsilon = \beta/4\tan\theta\ (10^{-3}), \tag{5}$$

where β is the FWHM of the most intense XRD peak. The micro-strain of prepared nanoparticle is found from the following equation:

$$\text{Micro-strain} = (\beta\cos\theta)/4\ (10^{-3}). \tag{6}$$

Dislocation density of the synthesized ferrite is calculated from the equation

$$\delta = 1/D^2\ (10^{15}), \tag{7}$$

where D represents the crystalline size. Stacking fault is calculated for the prepared ferrite samples with the help of the following formula:

$$\text{Stacking fault (SF)} = 2\pi^2/45\sqrt{3}(\tan\theta). \tag{8}$$

Stacking fault fluctuates repeatedly: first it decreases then it increases to a certain value and in the end it again decreases and then increases. This inhomogeneous behavior can be due to annealing temperature.[37] Table 1 shows all the structural parameters dependent on the doping concentration.

Table 1. Structural parameters of $Co_{0.5}Cd_{0.5}Bi_xFe_{2-x}O_4$ ($x = 0.0$, 0.05, 0.1, 0.15, 0.2, and 0.25).

Parameter	$x=0.0$	$x=0.05$	$x=0.1$	$x=0.15$	$x=0.2$	$x=0.25$
Crystalline size/nm	15.4157	14.1147	14.8737	11.7253	12.8087	13.4281
Lattice constant a/Å	8.50931	8.4783	8.46595	8.49676	8.49952	8.4948
Cell volume (a^3)	616.145	609.433	606.774	613.422	614.020	612.998
x-ray density/g·cm^{-3}	5.63509	5.86405	6.05738	6.15756	6.31720	6.49367
Bulk density/g·cm^{-3}	1.17301	1.26855	1.35518	1.24530	1.24331	1.27261
Lattice strain/10^{-3}	7.49341	8.15242	7.72146	9.84644	9.006118	8.593068
Microstrain/10^{-3} (lines^{-2}/m^{-4})	2.24769	2.45487	2.32960	2.95514	2.70519	2.580409
Dislocation density/10^{15} (lines/m^2)	4.20794	5.01940	4.52018	7.27363	6.09522	5.54588
Stacking fault	0.45118	0.45022	0.44974	0.45104	0.45083	0.45090

3.3. FTIR analysis

Fourier transform infrared spectrum (FTIR) is recorded the on iS50 FT-IR for further detailed analysis of crystal structure. The spinel structures of the prepared ferrites having compositional formula $Co_{0.5}Cd_{0.5}Bi_xFe_{2-x}O_4$ ($x = 0.0$, 0.05, 0.1, 0.15, 0.2, and 0.25) are investigated. The two frequency bands are recorded: one is high frequency bands ν_1 (at around 500 cm^{-1}) because of tetrahedral site of intrinsic stretching vibrations, and the other is low frequency band which is ν_2 (at around 400 cm^{-1}) because of octahedral stretching bands. These frequency bands represent the characteristic feature of spinel structure.[26,38] The changes in ν_1 are observed in a span of 530 cm^{-1}–538 cm^{-1} whereas ν_2 remains static. The high frequency band and low frequency band are formed because of the Fe^{3+}–O^{2-} stretching vibrations at tetrahedral and octahedral site. The shifting of ν_1 frequency band slightly to the high frequency is due to the variation generated in lattice parameter, and these changes affect the stretching vibrations of Fe^{3+}–O^{2-} due to which the band position may be changed.[24,26] Figure 3 shows the FTIR spectra observed in 400 cm^{-1}–1000 cm^{-1} range.

From the frequency band data the force constants are also calculated, which are K_t and K_o for tetrahedral and octahedral sites by the following formulas:

$$K_o = 0.942128M(\nu_2)^2/(M+32), \tag{9}$$

$$K_t = \sqrt{2}K_o\nu_1/\nu_2, \tag{10}$$

where M denotes the molecular weight, ν_1 and ν_2 are frequency bands. The force constants are analyzed to enhance the doping concentration, which indicates the possible strengthening of interionic bonding.[39] The tetrahedral radius and the octahedral radius are also obtained from the following formulas:

$$R_{tetra} = a\sqrt{3}(u-0.25) - R_o, \tag{11}$$

$$R_{octa} = a(5/8-u) - R_o, \tag{12}$$

where R_{tetra} is the tetrahedral radii, R_{octa} is the octahedral radii, u is the oxygen position parameter, and a represents the lattice parameter. The value of oxygen position parameter is 0.375 for FCC structure.[40]

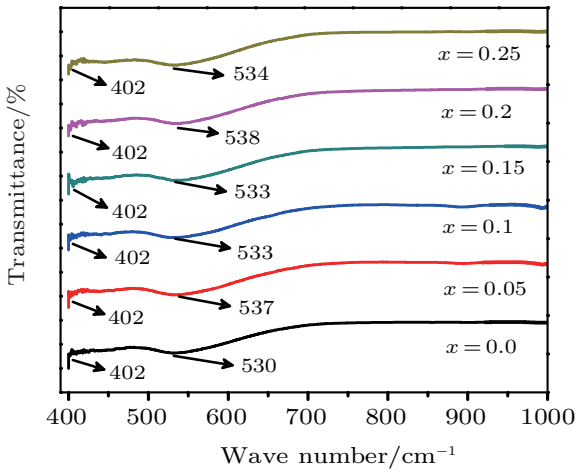


Fig. 3. FTIR analysis of $Co_{0.5}Cd_{0.5}Bi_xFe_{2-x}O_4$ ($x = 0.0$, 0.05, 0.1, 0.15, 0.2, and 0.25).

These tetrahedral and octahedral radii are seen to decrease inhomogenously, which proves the decrease in bond length with the concentration of Bi^{3+} increasing.[24] The values of these parameters are given in Table 2.

Table 2. Different parameters of FTIR analysis.

Parameters	$x = 0.0$	$x = 0.05$	$x = 0.1$	$x = 0.15$	$x = 0.2$	$x = 0.25$
Molecular weight/(gm/mol)	261	269	276	284	291	299
ν_1/cm^{-1}	530	537	533	533	538	534
ν_2/cm^{-2}	402	402	402	402	402	402
$K_o/(dyne/cm^2) \times 10^5$	1.35644	1.36066	1.36467	1.36850	1.37213	1.37561
$K_t/(dyne/cm^2) \times 10^5$	2.52909	2.57048	2.55886	2.56602	2.59698	2.58419
R_o	0.80733	0.79958	0.79649	0.80419	0.80488	0.8037
R_t	0.52232	0.51561	0.51293	0.5196	0.5202	0.51918

3.4. Dielectric properties

The dielectric properties of prepared ferrite samples having general formula of composition $Co_{0.5}Cd_{0.5}Bi_xFe_{2-x}O_4$ ($x = 0.0$, 0.05, 0.1, 0.15, 0.2, and 0.25) are calculated with the help of impedance analyzer in a span of frequency from 1 MHz to 3 GHz at room temperature (as shown in Table 3). The dielectric properties are of great interest because of their suitability in high frequency appliances. These properties strictly depend on the synthesis method, composition of material, and the cation positioning.[26] In order to obtain the information about conduction mechanism and polarization, the AC conductivity and the real and imaginary part of dielectric constant must be studied in a high frequency range.[41]

Table 3. Dielectric parameters for $Co_{0.5}Cd_{0.5}Bi_xFe_{2-x}O_4$ ($x = 0.0$, 0.05, 0.1, 0.15, 0.2 and 0.25).

Parameters	Frequency	$x = 0.0$	$x = 0.05$	$x = 0.1$	$x = 0.15$	$x = 0.2$	$x = 0.25$
Dielectric constant	1 MHz	4.74	3.69	2.86	5.07	2.53	2.49
	1 GHz	4.02	2.63	2.20	3.45	1.83	2.18
	3 GHz	4.18	2.49	2.17	3.55	1.73	2.18
Dielectric loss	1 MHz	0.163	0.113	0.110	1.18	0.419	0.315
	1 GHz	0.149	0.0250	0.0291	0.0702	0.00977	0.0213
	3 GHz	0.359	0.00308	0.0623	0.230	0.00203	0.0793
Tan loss	1 MHz	0.0344	0.0307	0.0385	0.232	0.165	0.126
	1 GHz	0.0372	0.00951	0.0132	0.0204	0.00534	0.0097
	3 GHz	0.0858	0.00124	0.0287	0.0646	0.00117	0.0364

3.4.1. Dielectric constant, dielectric loss and tangent loss

Dielectric constant, dielectric loss, and tangent loss of $Co_{0.5}Cd_{0.5}Bi_xFe_{2-x}O_4$ ($x = 0.0$, 0.05, 0.1, 0.15, 0.2, and 0.25) are calculated with respect to the frequency of applied field.

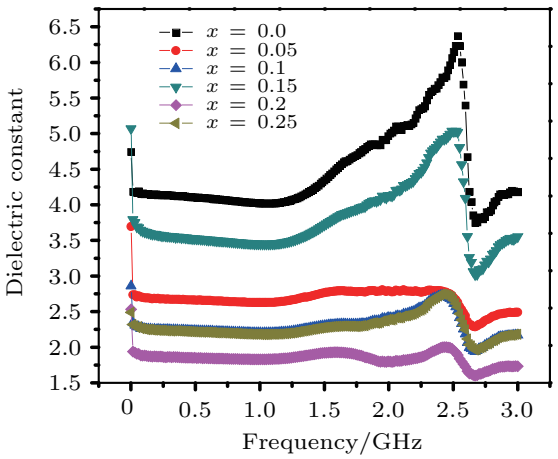


Fig. 4. Variations of dielectric constant *versus* frequency.

Figures 4 and 5 show these parameters as a function of frequency. These graphs exhibit the dispersion behaviors at high frequencies, such a kind of behavior is because of Maxwell Wagner interfacial polarization and also Koop's phenomenological theory. These models explain that the grain boundaries are more active at low frequencies whereas grains are more operational at high frequencies. While annealing the samples, the irregular spreading of oxygen ion at grains and grain boundaries lead to the ionic and electronic polarization at high frequency and the interfacial polarization at low frequency. As the frequency rises, the polarization goes on decreasing in strength and hence the dielectric constant continues to decrease. As is well known, the main charge carriers in ferrites are electrons, the electronic exchange occurs between Fe^{3+} and Fe^{2+} which reside at octahedral sites. This process of electronic exchange is known as electron hopping. This behavior of dielectric constant decreasing is accomplished due to the electron hopping because it does not obey the pattern of applied alternating field at very high frequency.[24,42–44]

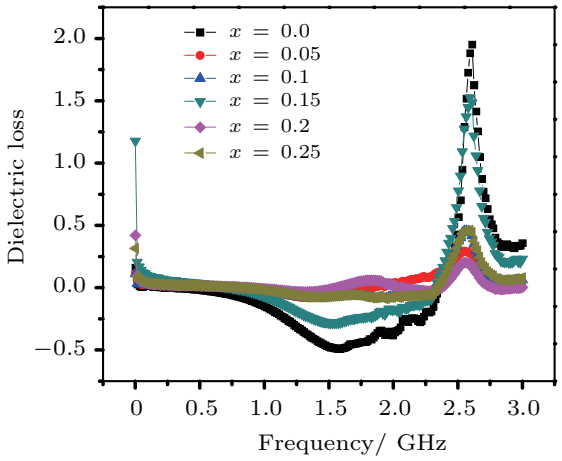


Fig. 5. Variations of dielectric loss *versus* frequency.

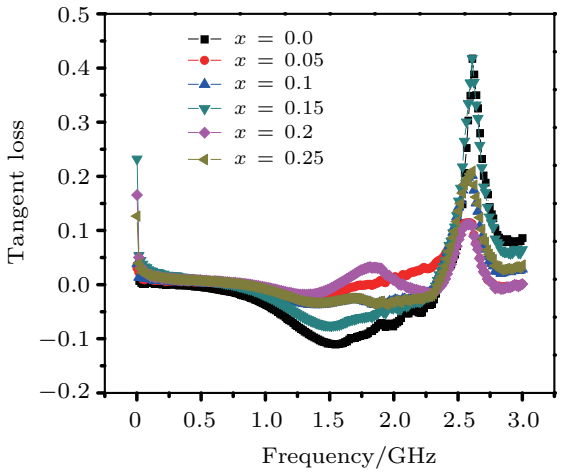


Fig. 6. Tangent loss *versus* frequency.

Figure 6 shows the variations in tangent loss with frequency. This variation in tangent loss is analyzed to be like that in dielectric constant and dielectric loss. In a feeble frequency range the electron hopping frequency follows the applied field frequency, that is why the loss is calculated to be comparatively high, but as soon as frequency of applied field

is enhanced further the electron hopping cannot follow the applied field frequency. Therefore after certain critical frequency, the tangent loss decreases significantly.[24] These dielectric parameters are listed in Fig. 3.

3.4.2. AC Conductivity

The AC conductivity is one of the important characteristics of dielectric material. The AC conductivity of the prepared ferrite samples $Co_{0.5}Cd_{0.5}Bi_xFe_{2-x}O_4$ (x = 0.0, 0.05, 0.1, 0.15, 0.2, and 0.25) are calculated in a frequency range from 1 MHz to 3 GHz. ssThe formula to be used for the calculation of AC conductivity is

$$\sigma_{ac} = (t/A) \cdot z'/(z'^2 + z''^2),$$

where t represents the thickness of pallet, A is its area, z' and z" represent the real and imaginary impedance parts, respectively. The plot of AC conductivity *versus* frequency for each of prepared samples is shown in Fig. 7.

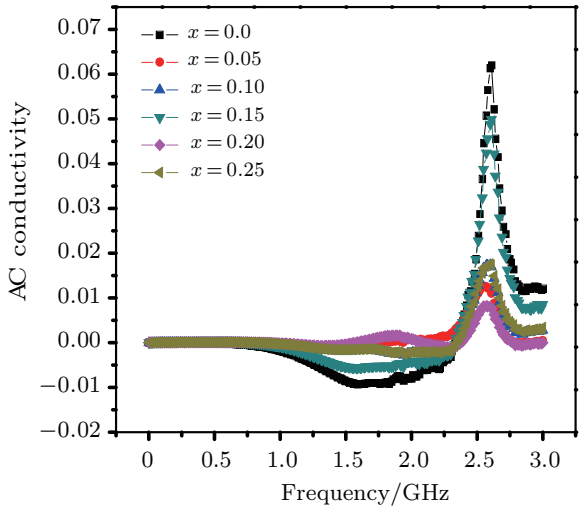


Fig. 7. AC Conductivity *versus* frequency.

From the figure it can be observed that for most of samples the AC conductivity has an increasing trend in the low frequency range, whereas in the high frequency range it presents the dispersive behavior . Maxwell–Wagner model and Koop's phenomenological theory both explain that the ferrites materials have high conducting grains which are separated by grain boundaries having resistive nature.[45] At low frequency the behaviors of all samples seem to be planar and the same due to high resistance of grain boundaries. At high frequencies, as a result of the effects of grains and the hopping phenomena in Fe^{2+} and Fe^{3+} at octahedral sites, the conductivity is enhanced. The increasing behavior of conductivity may also be due to the reduction of porosity. At low frequencies it is seen that the conductivity has a grain boundary effect whereas in the high frequency range the conducting effects of grains are observed, therefore the dispersion trend can be seen.[1,24,26]

3.4.3. Real and imaginary impedance

Impedance analysis is a powerful tool to relate dielectric properties of synthesized material with its microstructural composition.[46,47] The real and imaginary impedance part are calculated for each of the ferrite $Co_{0.5}Cd_{0.5}Bi_xFe_{2-x}O_4$ (x = 0.0, 0.05, 0.1, 0.15, 0.2, and 0.25). These impedance parts dependent on the applied field frequency are calculated as depicted in Figs. 8 and 9.

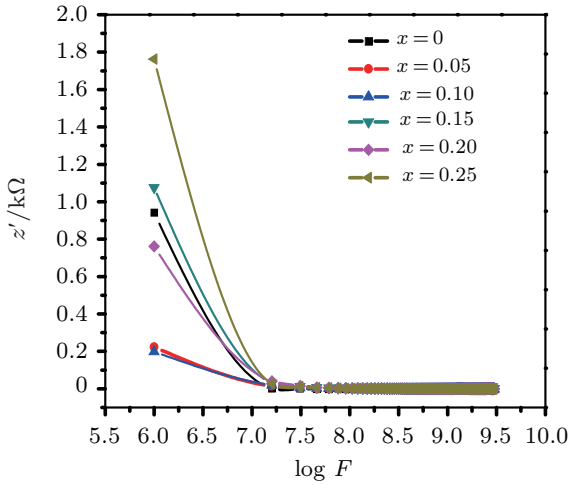


Fig. 8. Real part of impedance *versus* log of frequency.

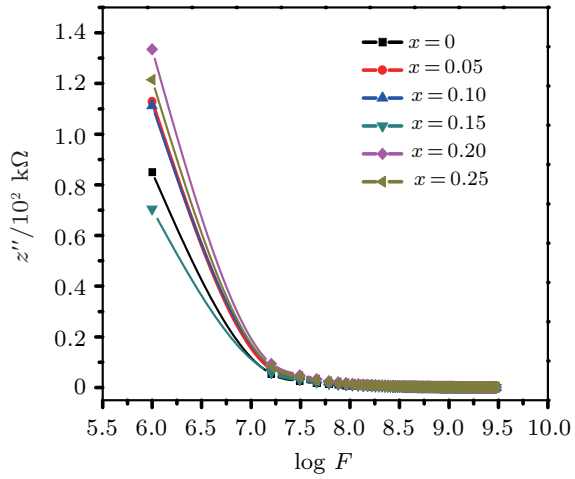


Fig. 9. Imaginary part of impedance *versus* log of frequency.

Impedance spectrum shows that the increase of applied frequency reduces the real and imaginary impedance parts. With the further increase of frequency the impedance curves of all samples merge with each other and at higher frequency impedance show constant behavior, which is attributed to the release of space charges.[48] These space charges are produced because of the disparity of concentration and also due to the inhomogeneity of applied field which tends to accumulate these charges on the grain boundaries. The decreasing real and imaginary impedance parts show the improvement of conductivity with the increase of field frequency.[47,48]

3.4.4. The real, imaginary modulus, and Cole–Cole (Nyquist) diagram interpretation

Real and imaginary modulus of the prepared ferrite having compositional formula $Co_{0.5}Cd_{0.5}Bi_xFe_{2-x}O_4$ ($x = 0.0$, 0.05, 0.1, 0.15, 0.2, and 0.25) are calculated as a function of applied frequency. The relations used for the calculation of real and imaginary modulus are

$$M' = \frac{\varepsilon'}{\varepsilon'^2 + \varepsilon''^2}, \tag{13}$$

$$M'' = \frac{\varepsilon''}{\varepsilon'^2 + \varepsilon''^2}. \tag{14}$$

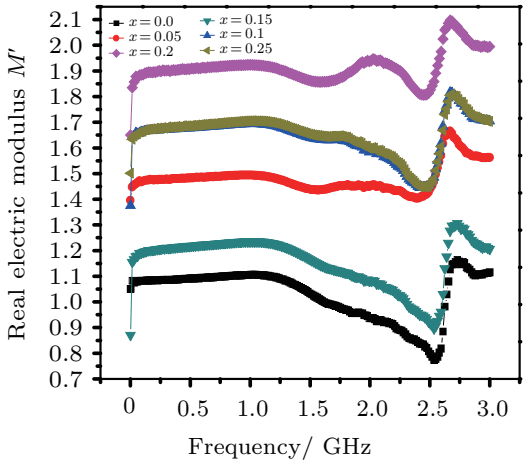


Fig. 10. Real electric modulus *versus* frequency graph.

Figures 10 and 11 demonstrate the plots of real and imaginary electric modulus *versus* applied field frequency in a range from 1 MHz to 3 GHz. The ferroelectric materials have an electrical response which can be analyzed by using electric modulus, and this electrical response is based on the phenomenon of electric polarization. In some of homogenous materials the bulk (grain) and grain boundary effects can be described on the basis of complex electric modulus formalism. Electric modulus is used to analyze the behavior of interfacial polarization depending on the applied field frequency in $Co_{0.5}Cd_{0.5}Bi_xFe_{2-x}O_4$.

If the grain boundary region occupies a greater volume, then the graph between M' and M'' can provide good information about the semicircle.[49] This kind of attitude is confirmed by obtaining the relation between grain boundary and the formation of peak.[1] The appearance of each peak vs. frequency in imaginary electric modulus is depicted in Fig. 11. The values of AC conductivity, impedance and modulus are represented in Table 4.

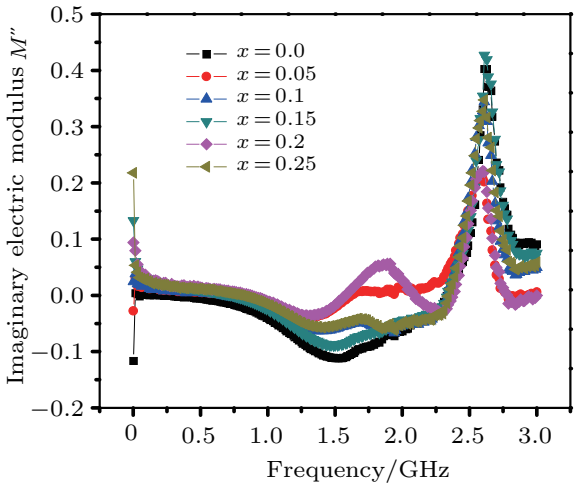


Fig. 11. Imaginary electric modulus *versus* frequency graph.

Table 4. AC conductivity, impedance, and modulus values for $Co_{0.5}Cd_{0.5}Bi_xFe_{2-x}O_4$ ($x = 0.0$, 0.05, 0.1, 0.15, 0.2, and 0.25) in the frequency range from 1 MHz to 3 GHz.

Parameters	Frequency	$x = 0.0$	$x = 0.05$	$x = 0.1$	$x = 0.15$	$x = 0.2$	$x = 0.25$
AC Conductivity	1 MHZ	5.79866×10^{-6}	7.87803×10^{-7}	7.2124×10^{-7}	9.54509×10^{-6}	1.91567×10^{-6}	5.26607×10^{-6}
	1 GHZ	1.883699×10^{-3}	3.96262×10^{-4}	4.596×10^{-4}	9.48×10^{-4}	1.6695×10^{-4}	3.30598×10^{-4}
	3 GHZ	1.2092363×10^{-2}	4.14805×10^{-4}	2.84216×10^{-3}	8.553363×10^{-3}	3.5165×10^{-6}	3.395429×10^{-3}
z'/Ω	1 MHZ	9.41×10^{3}	2.23×10^{3}	1.98×10^{3}	1.08×10^{4}	7.61×10^{3}	1.76×10^{4}
	1 GHZ	3.31	1.27	1.90	2.08	8.88×10^{-1}	1.38
	3 GHZ	2.45	1.64×10^{-1}	1.34	2.02	2.26	1.59
z''/Ω	1 MHZ	8.50×10^{4}	1.13×10^{5}	1.11×10^{5}	7.04×10^{4}	1.33×10^{5}	1.21×10^{5}
	1 GHZ	8.89×10^{1}	1.20×10^{2}	1.36×10^{2}	9.93×10^{1}	1.55×10^{2}	1.37×10^{2}
	3 GHZ	3.01×10^{1}	4.21×10^{1}	4.60×10^{1}	3.25×10^{1}	5.38×10^{1}	4.59×10^{1}
M'	1 MHZ	1.05039	1.39519	1.37548	0.870514	1.650339	1.501691
	1 GHZ	1.10524	1.493224	1.694277	1.234792	1.923289	1.705278
	3 GHZ	1.11549	1.562217	1.704708	1.205494	1.994711	1.703632
M''	1 MHZ	0.11640	0.027573	0.024533	0.13304	0.094080	0.217934
	1 GHZ	0.04118	0.015793	0.023585	0.025844	0.011037	0.017183
	3 GHZ	9.074×10^{-2}	6.065×10^{-3}	4.9524×10^{-2}	7.4754×10^{-2}	8.3825×10^{-5}	5.9111×10^{-2}

The Cole–Cole diagram is shown in Fig. 12, which provides the information about grain and grain boundaries. This graph can be plotted on any of these parameters such as electric modulus, permittivity and impedance. These parameters are interrelated to each other in terms of characteristics. The Cole–Cole plot shows only single semicircle, which confirms that the conduction behavior is due to grain boundaries only. Furthermore, the complex modulus spectra show that M'' is inversely related to the capacitance due to the fact that the bulk (grain) effects are also seen. The variations in the semicircle radius may be due to the substitution of Bi^{3+}. The obtained spectra can be explained by jump relaxation model (JRM) as well. According to this model, the conduction process at low frequency is due to successful hopping of charge carriers between A site and B site but this hopping mechanism is greatly restricted at high frequency, so the dispersion behavior is observed.[1,50]

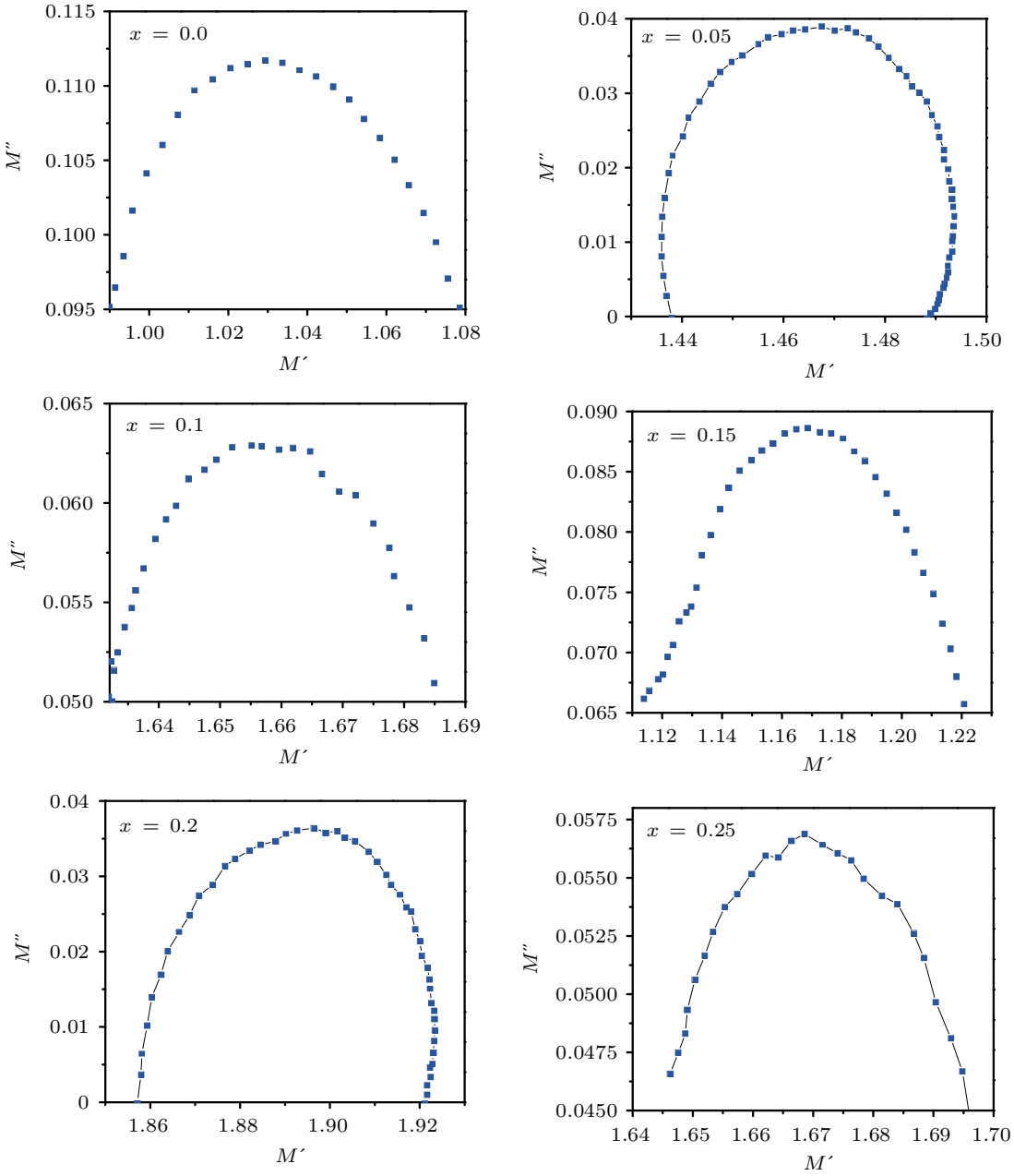


Fig. 12. Cole–Cole plot variations for $Co_{0.5}Cd_{0.5}Bi_xFe_{2-x}O_4$ ferrite ($x = 0.0$, 0.05, 0.1, 0.15, 0.2, and 0.25).

4. Conclusions

Nano-crystalline ferrites with general formula $Co_{0.5}Cd_{0.5}Bi_xFe_{2-x}O_4$ ($x = 0.0$, 0.05, 0.1, 0.15, 0.2, and 0.25) are effectively synthesized by the micro-emulsion method which has proved to be an easiest method of synthesizing such ferrites. The XRD studies confirm the FCC spinel structure with the appearance of sharp peaks. Crystalline size is found to be in nanosize range from 11 nm to 15 nm and is calculated by Debye–Scherrer formula. Lattice constant shows the decreasing behavior with Bi^{3+} substitution increasing due to

the replacement of large-radius Fe^{3+} ion by smaller-radius Bi^{3+} ion. Two frequency stretching bands are observed by FTIR studies, which are corresponding respectively to tetrahedral and octahedral site and are the characteristic bands of spinel structure. The weight loss of the ferrite material is calculated by TGA and DTA analyses, which shows the percentage weight loss of about 1.98% in a specified temperature range due to the evaporation of moisture and impurity content. Dielectric studies are carried out in a frequency range of 1 MHz–3 GHz, which follows the Maxwell Wagner model, and reveal the dielectric parameters decreasing with applied field frequency increasing. The AC conductivity of material is found to increase with frequency increasing due to the grain effect at high frequency. The impedance analysis shows decreasing tendency which in turn results in an increasing conductivity of material. It is attributed to the grain boundary effect. The real and imaginary modulus analysis conduces to the understanding of the bulk and grain boundary effect and the Cole–Cole explanation reveals the formation of single semicircle that confirms that the conduction mechanism is due to the grain boundaries at low frequency. These dielectric properties propose the probable usage of these nano-ferrites in high frequency applications, microwave applications, storage media, and semiconductor devices.

Acknowledgement

Authors thank the ORIC of Balochistan University of Information Technology Engineering and Management Sciences (BUITEMS) Quetta-PK, for help and financial support to accomplish this research work in the Department of Physics.

References

[1] Iqbal M A, Islam M U, Ali I, Khan M A, Sadiq I and Ali Ihsan 2014 *J. Alloys Compd.* **586** 404
[2] Yafet Y and Kittel C 1952 *Phys. Rev.* **87** 290
[3] Jiang J, Yang J M and Li L C 2007 *Physica B: Condens. Matter* **399** 105
[4] Wang Z, Jiang W, Li S X and Tong J S 2016 *Nucl. Instrum. Methods Phys. Res. B* **366** 1
[5] Wang K, Si N, Zhang Y L, Guo A B and Jiang W 2019 *Vacuum* **165** 105
[6] Wang K, Jiang W, Chen J N and Huang J Q 2016 *Superlattices and Microstructures* **97** 116
[7] Li M J, Xu Z P, Li Z B, Chen Y, Guo J W, Huo H M, Zhou H Y, Huangfu H C, Cao Z H and Wang H Y 2016 *Crystal Research and Technology* **51** 696
[8] Fu Y P, Hung D S and Yao Y D 2009 *Ceram. Int.* **35** 2179
[9] Al-Hilli M F, Li S and Kassim K S 2012 *J. Magn. Magn. Mater.* **324** 873
[10] Singh R P and Venkataraju C 2018 *Chin. J. Phys.* **56** 2218
[11] Zi Z F, Sun Y P, Zhu X B, Yang Z R, Dai J M and Song W H 2009 *J. Magn. Magne. Mater.* **321** 1251
[12] Grigorova M, Blythe H J, Blaskov V, *et al.* 1998 *J. Magn. Magn. Mater.* **183** 163
[13] Shenker H 1957 *Phys. Rev.* **107** 1246
[14] Reddy C V, Prabhakar Vattikuti S V, Ravikumar R V S S, *et al.* 2015 *J. Magn. Magn. Mater.* **394** 70
[15] Salunkhe A B, Khot V M, Phadatare M R and Pawar S H 2012 *J. Alloys Compd.* **514** 91
[16] Maaz K, Mumtaz A, Hasanain S K and Ceylan A 2007 *J. Magn. Magn. Mater.* **308** 289
[17] Naidek K P, Bianconi F, da Rocha T C R, *et al.* 2011 *J. Colloid Interf. Sci.* **358** 39
[18] Cedeño-Mattei Y and Perales-Pérez O 2009 *Microelectron. J.* **40** 673
[19] Fannin P C, Marin C N, Malaescu I, *et al.* 2011 *Mater. Design* **32** 1600
[20] Zhang Y, Yang Z, Yin D, Liu Y, Fei C L, Xiong R, Shi J and Yan G L 2010 *J. Magn. Magn. Mater.* **322** 3470
[21] Sajjia M, Oubaha M, Prescott T and Olabi A G 2010 *J. Alloys Compd.* **506** 400
[22] Singhal S, Jauhar S, Lakshmi N and Bansal S 2013 *J. Mol. Struct.* **1038** 45
[23] Prabhakar Vattikuti S V, Byon C, Shim J, *et al.* 2015 *J. Magn. Magn. Mater.* **393** 132
[24] Junaid M, Khan M A, Iqbal F, *et al.* 2016 *J. Magn. Magn. Mater.* **419** 338
[25] Mohanty V, Cheruku R, Vijayan L and Govindaraj G 2014 *J. Mater. Sci. Technol.* **30** 335
[26] Gilani Z A, Warsi M F, Khan M A, *et al.* 2015 *Physica E* **73** 169
[27] Sun C and Sun K 2007 *Physica B: Condens. Matter* **391** 335
[28] Motavallian P, Abashtb B, Mirzaeea O and Abdollah-Pour H 2019 *Chin. J. Phys.* **57** 6
[29] Wang J P, Chen Q D, Li S L, Ji Y J, Mu W Y, Feng W W, Zeng G J, Liu Y W and Liang E J 2018 *Chin. Phys. B* **27** 066501
[30] Ali R, Mahmood A, Khan M A, *et al.* 2014 *J. Alloys Compd.* **584** 363
[31] Lodhi M Y, Mahmood K, Mahmood A, *et al.* 2014 *Curr. Appl. Phys.* **14** 716
[32] Gowreesan S and Kumar A R 2018 *Chin. J. Phys.* **56** 1262
[33] Iqbal M A, Islam M, Ashiq M N, *et al.* 2013 *J. Alloys Compd.* **579** 181
[34] Anjum S, Sehar F, Bashir F, Awan M S and Mustafa Z 2015 *Mater. Today* **2** 5182
[35] Chavan P, Naik L R, Belavi P B, Chavan G N and Kotnala R K 2017 *J. Alloys Compd.* **694** 607
[36] Chandrasekaran G, Selvanandan S and Manivannane K 2004 *J. Mater. Sci.* **15** 15
[37] Brightlin B and Balamurugan S 2016 *Appl. Nanosci.* **6** 1199
[38] Ghasemi A and Mousavinia M 2014 *Ceram. Int.* **40** 2825
[39] Karimi Z, Mohammadifar Y, Shokrollahi H, *et al.* 2014 *J. Magn. Magn. Mater.* **361** 150
[40] Hemeda O 2004 *Turkish J. Phys.* **28** 121
[41] Orak I, Kocyigit A and Alindal Ş 2017 *Chin. Phys. B* **26** 028102
[42] Khan M A, Sabir M, Mahmood A, *et al.* 2014 *J. Magn. Magn. Mater.* **360** 188
[43] Singh N, Agarwal A and Sanghi S 2011 *Curr. Appl. Phys.* **11** 783
[44] Shkir M, Ganesh V, AlFaify S, Yahia I S and Anis M 2018 *Chin. Phys. B* **27** 054216
[45] Jalaiah K, Babub K V, Babu K R, *et al.* 2018 *Chin. J. Phys.* **56** 2039
[46] Yadav R S, Kuřitka I, Vilcakova J, *et al.* 2017 *Adv. Nat. Sci.* **8** 045002
[47] Costa M M, Pires G F M Jr, Terezo A J, Graça M P F and Sombra A S B 2011 *J. Appl. Phys.* **110** 034107
[48] Joshi J H, Kanchan D K, Joshi M J, Jethva H O and Parikh K D 2017 *Mater. Res. Bull.* **93** 63
[49] Rodrigues H O, Junior G F M P, Sales A J M, *et al.* 2011 *Physica B: Condens. Matter* **406** 2532
[50] Sujatha C, Reddy K V, Babu K S, *et al.* 2013 *J. Phys. Chem. Solids* **74** 917